RSC Advances

PAPER

Morphology controlled nano-structures of an octa(phenoxy)-substituted phthalocyaninato zinc complex: solvent effect on the self-assembly behaviour†

Cite this: *RSC Adv.*, 2014, **4**, 14807

Xia Zhang,[a] Dameng Gao,[a] Jian Gao,[a] Peihua Zhu,[a] Marcel Bouvet[b] and Yanli Chen*[a]

Received 27th August 2013
Accepted 10th March 2014

DOI: 10.1039/c3ra44687e

www.rsc.org/advances

The 2,3,9,10,16,17,24,25-octakis(phenoxy)phthalocyaninato zinc, (Zn[Pc(OPh)$_8$]) was fabricated into nano-/micro-structures *via* solution-phase self-assembly. The self-assembling properties of Zn[Pc(OPh)$_8$] in coordinating and non-coordinating solvents (methanol and *n*-hexane) have been comparatively studied by electronic absorption, fluorescence, Fourier transform infrared spectroscopy (FT-IR), scanning electronic microscopy (SEM), X-ray photoelectron spectroscopy (XPS) and X-ray diffraction (XRD) techniques. The conducting properties were evaluated by current–voltage (*I*–*V*) measurements. Due mainly to the presence of different intermolecular Zn–O coordination interactions between the Zn[Pc(OPh)$_8$] molecules in *n*-hexane and between the Zn[Pc(OPh)$_8$] and solvent molecules in methanol, the self-assembly of the Zn[Pc(OPh)$_8$] results in nano-/micro-structures with distinctly different morphology as follows: nanobelts in *n*-hexane, and soft nano-sticks, microscale needle mushroom as well as pine leaves in methanol depending on aggregation time. The size and/or morphological evolution of the nanostructures have been clearly revealed during the self-assembly process. The present result appears to represent the first effort toward realization of controlling and tuning the biomorphs of self-assembled nanostructures of phthalocyanine-related complexes through the solvent coordinating effect. Furthermore, both nanobelts and micrometer-sized pine leaves were revealed to show good semiconductor features.

Introduction

Recently, the self-assembly of functional organic molecules into well-defined structures has attracted considerable research interest due to their versatile applications in nanoscience and nanotechnology.[1,2] Depending on various non-covalent interactions including hydrogen bonding, hydrophilic/hydrophobic, electrostatic interaction, ionic bonding, metal coordination, van der Waals forces, π–π stacking and steric effects, a wide variety of nanostructures such as wires,[3] belts,[4] vesicles,[5] and tubes[6] have been fabricated from various functional molecules. Among which, conjugated molecular systems have been recognized as attractive building blocks for supramolecular self-assemblies towards construction of functional nanodevices. As the typical representative of functional molecular materials with their unique planar and rigid molecular geometry as well as aromatic electron delocalization over the molecular frame, metallophthalocyanines often exhibit intriguing, peculiar, and tunable spectroscopic, electrochemical, photophysical and assembly properties.[7–10] By virtue of these excellent features, a wide variety of sophisticated phthalocyanines-based self-assembled nano-structures, such as nanotubes, nanowires, nanosheets, nanorods, *etc.*, have been important potential applications in the fields of chemical sensors,[11–13] organic field transistor,[14] photovoltaic cells,[15] optical data storage,[16] photosensitizers in the photodynamic therapy,[17] nonlinear optics,[18] organic photoconductors.[19]

Investigations have revealed that the nanostructural morphology of these phthalocyanine derivatives are primarily governed by the peripheral substituents of the Pc ring and central metal atom.[2,11–21] For example, a series of mixed (phthalocyaninato)(porphyrinato) europium complexes having different number of porphyrin hydroxyphenyl groups leads to the formation of nanostructures with leaves, sheets, ribbons and spherical shape in the solution-phase self-assembly

[a]*Shandong Provincial Key Laboratory of Fluorine Chemistry and Chemical Materials, School of Chemistry and Chemical Engineering, University of Jinan, Jinan 250022, P. R. China. E-mail: chm_chenyl@ujn.edu.cn; Tel: +86-531-89736150*

[b]*Institut de Chimie Moléculaire de l'Université de Bourgogne, CNRS UMR 6302, Université de Bourgogne, Dijon, 21078, France*

† Electronic supplementary information (ESI) available: Synthesis details of Zn[Pc(OPh)]$_8$, fluorescence spectra of Zn[Pc(OPh)$_8$] and its self-assembled nanostructures (Fig. S1), X-ray photoelectron spectra of Zn[Pc(OPh)$_8$] and its self-assembled nanostructures (Fig. S2), the length and width distribution of the self-assembled Zn[Pc(OPh)$_8$] nanostructures (Fig. S3). See DOI: 10.1039/c3ra44687e

process.[2a] Phthalocyanines appended with substituted crown-ether moieties have been readily self-assembled into long fibres.[22] Cooperation between the π–π interaction and sulfur–sulfur and various metal–ligand coordination among the molecules of metal-free phthalocyanine derivative bearing alkylthio moieties and its copper and lead congeners induces the formation of nanobelts, nanoribbons and cluster nanoflowers.[20] The morphological transition from the helical ribbon structure to tubular superstructure of unsymmetrical metal-free phthalocyanine decorated with one peripheral dimethylaminoethyloxy side chain during the self-assembly process was displayed.[23] This, to the best of our knowledge, represents the sole example of nanostructures with the morphological transition observed from phthalocyanines. In general, great progress has been made in phthalocyanine-based material chemistry, and various self-assembly strategies for well-defined phthalocyanine-based nanostructures have been well established. However, it must be pointed out that most of these studies have mainly focused on the construction of various phthalocyanine-based nanostructures with well-defined morphologies through molecular design and synthesis, and few studies devoted to expatiating on the effect of solvent on aggregated structure. In this work, we report an unexpected solvent effect of coordinating and non-coordinating solvents (methanol and *n*-hexane) on the self-assembly of 2,3,9,10,16,17,24,25-octakis(phenoxy) phthalocyaninato zinc complex, Zn[Pc(OPh)$_8$], Scheme 1. This complex forms nanobelts in *n*-hexane, whereas in methanol it self-assembles into the nanostructures with the morphological evolution from soft nanosticks, needle mushroom to pine leaves with an increased aggregation time. The present result represents the first example of various phthalocyanine-related biomorphs obtained *via* biomorphic transitions using solution-based processing. In addition, nanobelts and micrometer-sized leaves were revealed to show good semiconductor features.

Results and discussion

Electronic absorption and fluorescence spectra

The electronic absorption of Zn[Pc(OPh)$_8$] in $CHCl_3$ and its aggregates fabricated in *n*-hexane and methanol are recorded as shown in Fig. 1. As can be seen, this complex in $CHCl_3$ shows a typical non-aggregated electronic absorption spectrum of monomeric metallophthalocyanines with the Soret band at 362 nm and the main Q band at 680 nm in combination with a weak vibronic shoulder at 614 nm (Fig. 1A).[20,24] When dispersed in *n*-hexane and methanol, the molecules of Zn[Pc(OPh)$_8$] undergo aggregation due to the limited solubility, which leads to distinctive change in its electronic absorption spectra (Fig. 1B and C). Obvious band broadening is observed due to the significantly intermolecular interaction in the self-assembled nanostructures. In comparison with that in $CHCl_3$, the Soret band of the nanostructures for Zn[Pc(OPh)$_8$] formed in *n*-hexane and methanol shows a significant red-shift from 362 to 398 and 382 nm, while the main Q absorption lose some intensity and red shifted from 680 nm to 805 and 796 nm, respectively. Such a spectral change implies the formation of J aggregates with a slipped co-facial arrangement of the Zn [Pc(OPh)$_8$] molecules in the nanostructures due to the strong exciton coupling.[20,25,26] It is worth noting that the red shifts for both the Soret and Q bands are more marked in the aggregates formed from *n*-hexane than those from methanol, indicating that stronger intermolecular interactions exist in the former than the latter due likely to the introduction of metal–ligand (Zn–O) coordination between the ether oxygen in the phenoxy group in one molecule and the core zinc of another molecule in the aggregates formed from *n*-hexane (as a non-coordinating solvent). In the case of the nanostructures formed in methanol (as a coordinating solvent), we proposed that complementary Zn–O coordination of the hydroxyl oxygen in solvated methanol molecule with zinc center of neighbouring phthalocyanine molecule *via* a weak Zn[Pc(OPh)$_8$]/CH_3OH complex. This kind of complementary coordination would lead to a relatively large separation between the neighbouring phthalocyanine rings, and in turn results in a relatively weak π–π interaction between neighbouring stacking phthalocyanine molecules in the direction perpendicular to the phthalocyanine rings. Further evidence for this point comes from fluorescence, FTIR, XRD and XPS results as detailed below.

The fluorescence spectra of complex Zn[Pc(OPh)$_8$] in chloroform, *n*-hexane and methanol are compared in Fig. S1 (ESI†). The fluorescence quantum yield of Zn[Pc(OPh)$_8$] is reduced

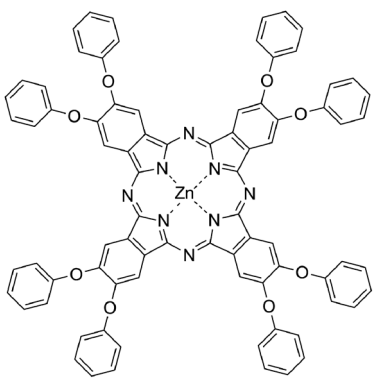

Scheme 1 Schematic structure of Zn[Pc(OPh)$_8$].

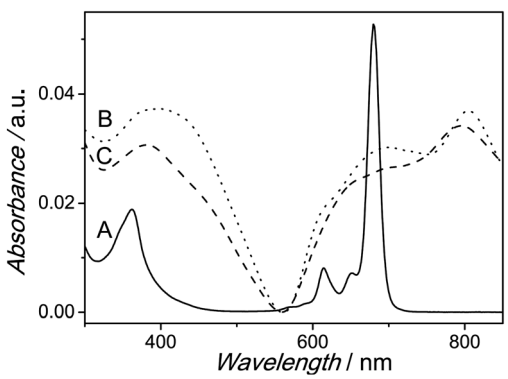

Fig. 1 Electronic absorption spectra of (A) Zn[Pc(OPh)$_8$] in chloroform (solid line), and its self-assembled nanostructures formed (B) in *n*-hexane (dot line) and (C) in methanol (dash line).

from 0.23 for the isolated Zn[Pc(OPh)$_8$] to about 0.0012 and 0.0044 upon aggregation in *n*-hexane and methanol, respectively, using zinc phthalocyanine ($\Phi_f = 0.30$) in benzene as a reference following a literature,[27] which is consistent with electronic coupling between the Pc rings formed by the interaction between adjacent Zn[Pc(OPh)$_8$] molecules in a slipped cofacial arrangement.[20,28] The higher fluorescence quantum yield observed for the nanostructures formed in methanol relative to that in *n*-hexane clearly suggests formation of aggregates with relatively weak π–π interactions between the phthalocyanine rings of Zn[Pc(OPh)$_8$], which is in agreement with a relatively low aggregation tendency due to the complementary Zn–O (CH_3OH) coordination interaction.

FT-IR spectra

The FT-IR spectra of Zn[Pc(OPh)$_8$] and its self-assembled nanostructures formed in *n*-hexane and methanol are shown in Fig. 2. As can be seen, almost all the vibration bands observed in the IR spectra of the nanostructures can be found in the spectrum of bulk Zn[Pc(OPh)$_8$], which unambiguously confirms the composition of two kinds of nanostructures. It is worth noting that the three bands appeared at approximately 891, 1207 and 1628 cm^{-1} for the bulk Zn[Pc(OPh)$_8$] due to ν(Zn–N), ν_s(C–O–C) and ν(C=N) stretching vibrations,[29,30] Fig. 2A, are broadened and shift to 845, 1203 and 1653 cm^{-1} in the self-assembled nanostructures formed in *n*-hexane (Fig. 2B), due to the formation of Zn–O metal–ligand coordination between ether oxygen in the phenoxy group in one phthalocyanine molecule and zinc center of neighboring phthalocyanine molecule in the nanostructure. However, in the case of self-assemble nanostructures formed in methanol (Fig. 2C), the peak frequencies for ν(Zn–N) and ν(C=N) modes shift to 881 and 1634 cm^{-1}, while the ν_s(C–O–C) (1207 cm^{-1}) band remains unchanged, in comparison with those of bulk Zn[Pc(OPh)$_8$]. With reference to previous singe crystal X-ray diffraction analysis for metallophthalocyanines and porphyrinato zinc complexes,[24,31] the complementary Zn–O coordination of the hydroxyl oxygen in solvated methanol molecule with zinc centre of neighboring phthalocyanine molecule might be responsible for the phenomena. In particular, a lower peak frequency for the ν(Zn–N) mode in the spectra of the nanostructures formed in *n*-hexane than that in methanol revealed that the Zn–O coordination from different electron donors has a great influence on the intermolecular interaction of self-assembled nanostructures.

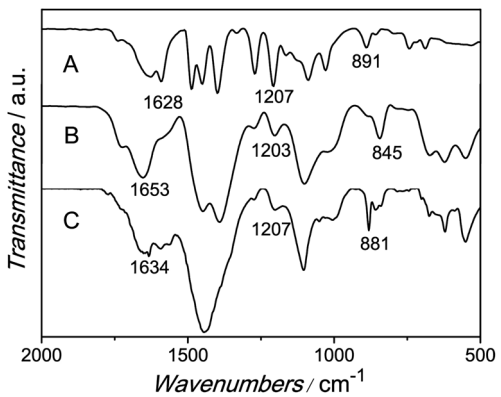

Fig. 2 IR spectra of (A) the bulk Zn[Pc(OPh)$_8$], its self-assembled nanostructures formed (B) in *n*-hexane and (C) in methanol, in the region of 500–2000 cm^{-1} with 2 cm^{-1} resolution.

X-ray diffraction patterns of the nanostructures

The internal structures of self-assembled aggregates of Zn[Pc(OPh)$_8$] are investigated by XRD analysis. As shown in Fig. 3A, the XRD diagram of the nanostructures formed in *n*-hexane shows one comparatively strong and sharp diffraction peak at $2\theta = 4.26°$ (corresponding to 2.07 nm) along with another weaker diffraction at $2\theta = 6.46°$ (1.37 nm) in the low angle range, which are ascribed to the diffractions from the (001) and (100) planes, respectively.[30,31] According to the single crystal X-ray diffraction analysis of analogue MnCl[Pc(OPh)$_8$],[25] the *d*-spacing of 2.07 and 1.37 nm could be attributed to the average length along the long axis of Zn[Pc(OPh)$_8$] and the thickness along the perpendicular direction to the tetrapyrrole rings, respectively, as shown in Fig. 4A. In the wide-angle range, the (001) plane also shows its series of higher order diffraction peaks at 1.01 (002), 0.703 (003), and 0.404 nm (005), respectively, which means that there exists very regular repetition of the nanostructure and one-dimensionally favorable growing orientation along the long axis of the Zn[Pc(OPh)$_8$]. Furthermore, the XRD pattern of Zn[Pc(OPh)$_8$] nanostructures formed from *n*-hexane presents additional diffraction at 0.423 and 0.316 nm, which can be attributed to the phenyl–phenyl distance between the phenyl π moieties of neighboring molecules[24] and the π–π stacking distance of phthalocyanine rings

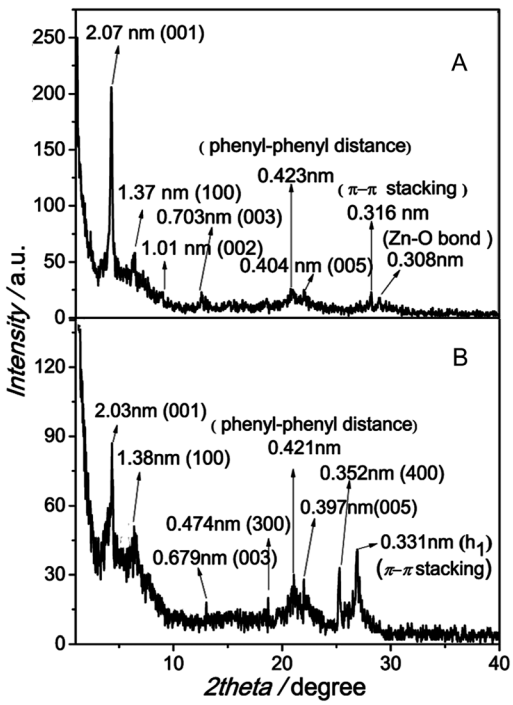

Fig. 3 X-ray diffraction patterns of the self-assembled nanostructures of Zn[Pc(OPh)$_8$] formed (A) in *n*-hexane and (B) in methanol.

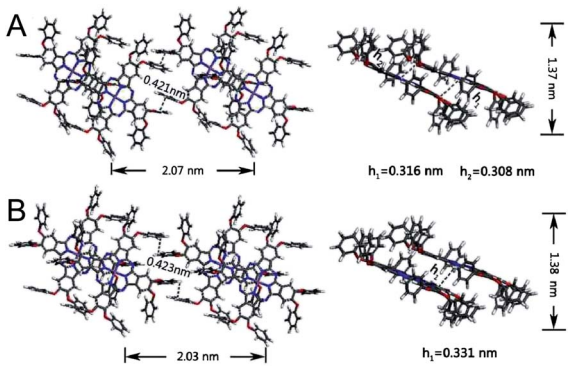

Fig. 4 Schematic representation in top view (left) and in side view (right) of the 2D packing diagram of the nanostructure formed (A) in *n*-hexane and (B) in methanol.

between the adjacent molecules, respectively,[23] whereas the relatively weaker diffraction at 0.308 nm is associated with the distance of a Zn–O coordination bond between the adjacent phthalocyaninato zinc molecule,[31] Fig. 4A. This is in good accordance with the results of electronic absorption and IR spectroscopy. The similar diffraction peaks in the low angle region from the (001) and (100) planes (at 2.03 and 1.38 nm) are also obtained for $Zn[Pc(OPh)_8]$ aggregates formed in methanol by comparison with those in *n*-hexane, Fig. 3B, implying the similar stacking mode (J aggregation) for the $Zn[Pc(OPh)_8]$ nanostructures in either coordinating or non-coordinating solvents. However, in the wide-angle range, both (001) and (100) planes all exhibit higher-order diffractions at 0.679 (003), 0.397 (005), 0.474 (300) and 0.352 nm (400). This indicates that the phthalocyanine rings are arranged two-dimensionally to form a layer structure coplanar to the phthalocyanine rings, and the phenoxy groups are used to connect them within the layer, Fig. 4B. Notably, in comparison with the π–π stacking distance of phthalocyanine rings between the adjacent molecules of Zn $[Pc(OPh)_8]$ nanostructures formed from *n*-hexane (0.316 nm), the observation of a larger stacking distance between neighboring molecules of nanostructures formed from methanol (0.331 nm) indicates decreasing intermolecular interaction between neighboring molecules of $Zn[Pc(OPh)_8]$ since the solvated methanol molecules get into the aggregates by complementary Zn–O coordination bonds. These findings confirm again the effect of the solvent on tuning the intermolecular interaction and in turn the favorable growing orientation of the nanostructures during the self-assembly process.

XPS analysis

To further confirm the difference of intermolecular Zn–O interactions in the resulting nanostructures, X-ray photoelectron spectroscopy (XPS) is employed to determine the environments of the zinc ions. Fig. S2 (ESI†) displays the XPS spectra of aggregates of $Zn[Pc(OPh)_8]$ formed in *n*-hexane and methanol, respectively. For comparison, another solid sample was prepared from the evaporation of a drop of $Zn[Pc(OPh)_8]$ $CHCl_3$ solution on the silicon surface (cast film). As expected, both the aggregates and cast film of $Zn[Pc(OPh)_8]$ show typical signals for the Zn^{2+} ion in their XPS spectra. The strong absorption peak at about 1022 eV and the weak absorption peaks at about 1045 eV for the cast film are attributed to Zn^{2+} $2p_{3/2}$ and Zn^{2+} $2p_{1/2}$, respectively.[20,32] However, the Zn^{2+} signals in the XPS spectrum of the aggregates fabricated from *n*-hexane undergo an obvious shift in the direction of lower binding energy compared those of the cast film and the aggregates from methanol, implying a change in Zn^{2+} environment after self-assembly in *n*-hexane due to the formation of relatively strong Zn–O coordination bonds in the aggregates. In contrast, no obviously chemical shift of the Zn^{2+} signals are observed for the aggregates formed in methanol compared to those of the cast film, implying very weak Zn–O coordination interaction between $Zn[Pc(OPh)_8]$ and solvated CH_3OH molecule, which is in good accordance with the results of XRD analysis.

Morphology of the aggregates

The foregoing X-ray studies suggest that $Zn[Pc(OPh)_8]$ in *n*-hexane should grow up to some one-dimensional (1D) aggregate, whereas $Zn[Pc(OPh)_8]$ in methanol should grow up to some two-dimensional (2D) aggregate. It is interesting to know whether these microscopic intermolecular interaction patterns are really reflected by the macroscopic superstructures. Fig. 5 shows SEM images of $Zn[Pc(OPh)_8]$ aggregates formed with different aggregation time. It is clearly seen that $Zn[Pc(OPh)_8]$ molecules in *n*-hexane assemble into a belt-like structure with an obviously increased length from about 1 to 4 μm and slightly increased width from about 100 nm to 160 nm as the self-assembly time was increased from 1 to 2 h, Fig. 5A and B, S3A and B, (ESI†). However, further prolong aggregation time being over 2 h (such as 24 h) does not distinctly induce further increase in the ratio of length over width for the belts, Fig. 5C. Consequently, the controlled shape and size with narrow

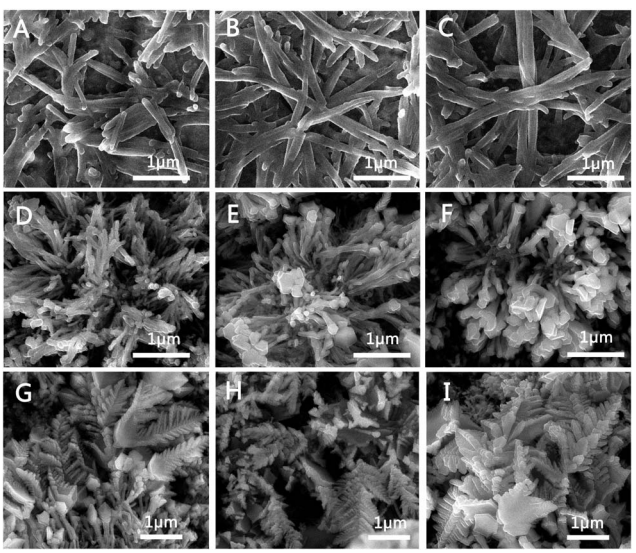

Fig. 5 SEM images of the morphologies self-assembled from *n*-hexane after (A) 1 h, (B) 2 h, (C) 24 h, and methanol after (D) 1 h, (E) 2 h, (F) 4 h, (G) 8 h, (H) 12 h, and (I) 24 h.

distribution for the belts have been achieved. These findings also suggest fast growth by molecular assembly to form uniform nano-belts. The strong Zn–O axial coordination between Zn[Pc(OPh)$_8$] molecules promotes the growth of aggregates, which continue to grow into a extended 1D belt in cooperation with π–π stacking interaction as well as lateral association of side groups among adjacent Zn[Pc(OPh)$_8$] molecules.[33] It is worth noting that the 1D nano-structures with controlled shape and size are highly desired for fabricating nano-scale molecular (opto)-electronic devices which often require a wide variety of channel lengths to achieve the optimum gate or optical modulation. Specifically, we find the Zn–O axial coordination among adjacent Zn[Pc(OPh)$_8$] molecules is important to form these 1D assemblies. Very interestingly, when methanol (coordinating solvent) was used as the poor solvent instead of *n*-hexane (non-coordinating solvent), defined one-dimensional self-assembled belts have not be obtained. Instead, the soft sticks, with about 1–2 μm in length and 50–100 nm in width are found for Zn[Pc(OPh)$_8$] aggregates formed in methanol after one hour of aggregation, Fig. 5 D, S3C and D, (ESI†). After 2 h aggregation, some nanosheets with diameter ranging from 200 to 300 nm formed on the top of some sticks, and several of which further pack together into a "needle mushroom"-like structure with almost the same length as soft sticks, as the aggregation time up to 4 h, Fig. 5E and F, S3E and F (ESI†).

Most interestingly, along with aggregation time prolonged to 8 h, adjacent nanosheets attached together gradually, which in turn construct well-defined "major stem" and branches spreading out from its stem, Fig. 5G. Finally, a clear "pine leaf"-like structure is archived after above 12 h, and the average length of the resulting pine leaves are still about 1 to 2 μm, which are the same as those of the original soft sticks at the early stage of aggregation, Fig. 5H, I and S3G (ESI†). The morphological evolution from soft nanosticks, needle mushrooms to pine leaves is achieved during the aggregating. Notably, this appears to represent the first example of three kind of phthalocyanine-related biomorphs obtained *via* biomorphic transitions using solution-based processing. The most closely related biomorphic structure previously observed is the microscale four-leaf clover formed by self-assembly of anionic and cationic porphyrins.[34] Accompanied by the information deduced from the UV-vis, fluorescence, IR and XPS spectra, the slow kinetics for the morphological transitions are mainly due to the influence of solvated molecules introduced into the aggregates by weak Zn–O association of the hydroxyl oxygen in solvated methanol molecule with zinc center of neighboring phthalocyanine molecule, which controlled the subtleties in self-assembly processes. Accordingly, the morphologies of the synthesized Zn[Pc(OPh)$_8$]-based nanomaterials were readily controlled by the selected solvent conditions and/or the aggregating time.

Assembly mechanism

On the basis of the experimental results described above, the formation process of the nanostructures in *n*-hexane and methanol was illustrated, Fig. 6. In *n*-hexane, Zn–O axial coordination between the central zinc ion of one Zn[Pc(OPh)$_8$] molecule and the oxygen atom of the adjacent molecule is expected to strengthen the intermolecular π–π interaction. This kind of J-type π–π stacking increases the intermolecular interaction and thus results in the formation of extended 1D nanobelts.[35] In contrast to the extended π stacks formed in *n*-hexane, the additional Zn–O (CH_3OH) coordination interaction for Zn[Pc(OPh)$_8$] in methanol weakened intermolecular π–π stacking, which limited the continuous growth of flat-elongated sticks along the perpendicular direction of phthalocyanine rings. As a result, the accumulation of surface free energy attributed to splaying of soft sticks, should eventually lead to significant curving and aggregation among the soft sticks, inducing the formation of the needle mushroom-like superstructures.[23,36] To further lower the energetic penalty from the edge of needle mushroom, the oriented attachment would go on to construct more complex pine leaf-like superstructure, which is the most stable morphology as evidenced by the observation of a morphological transition in Fig. 6.

I–V properties

The uniform aggregates of Zn[Pc(OPh)$_8$] with well-defined nanostructures would be promising candidates for applications in electronic devices. To demonstrate the potentials of these nanostructures, the diluted suspension of molecular aggregates of Zn[Pc(OPh)$_8$] formed in methanol and *n*-hexane was carefully dropped onto glass substrates with ITO interdigitated electrodes (IDEs), respectively. After complete evaporation of the solvents, the densely packed nanostructural films remained and adhere to ITO IDEs/glass substrate tightly, leading to the electron conductivity measurement *in situ*. For comparison, the cast film formed in chloroform was prepared by dropping Zn[Pc(OPh)$_8$] solution onto glass substrates with ITO IDEs. Fig. 7 shows the current–voltage (*I–V*) characteristics of nanobelts, nanoleaves and the cast film. The electronic conductivity is calculated to be around 2.4×10^{-7}, 4.5×10^{-8} and 6.78×10^{-9} S m^{-1} for the nanobelts, nanoleaves and the cast film, respectively (the experiments were repeated for more than three times on different pieces of films).[13,37] In particular, the nanobelts of Zn[Pc(OPh)$_8$] shown a much better conductivity in comparison to ultralong nanobelts self-assembled from perylene tetracarboxylic diimide[38] and polymer nanowires (*e.g.* polythiophene).[39] Furthermore, the effect of complementary coordination from a solvent on the morphological evolution of nanostructures, and in turn on the conductivity were revealed in the present case. The higher conductivity observed for the nanobelts than nanoleaves is consistent with their higher the one-dimensional order and enhanced π–π stacking by metal–ligand coordination bonding interaction among phthalocyanine molecules.[33,40,41]

Conclusion

We have demonstrated that distinctly different Zn[Pc(OPh)$_8$]-based nano-/micro-structures, including nanobelts, soft

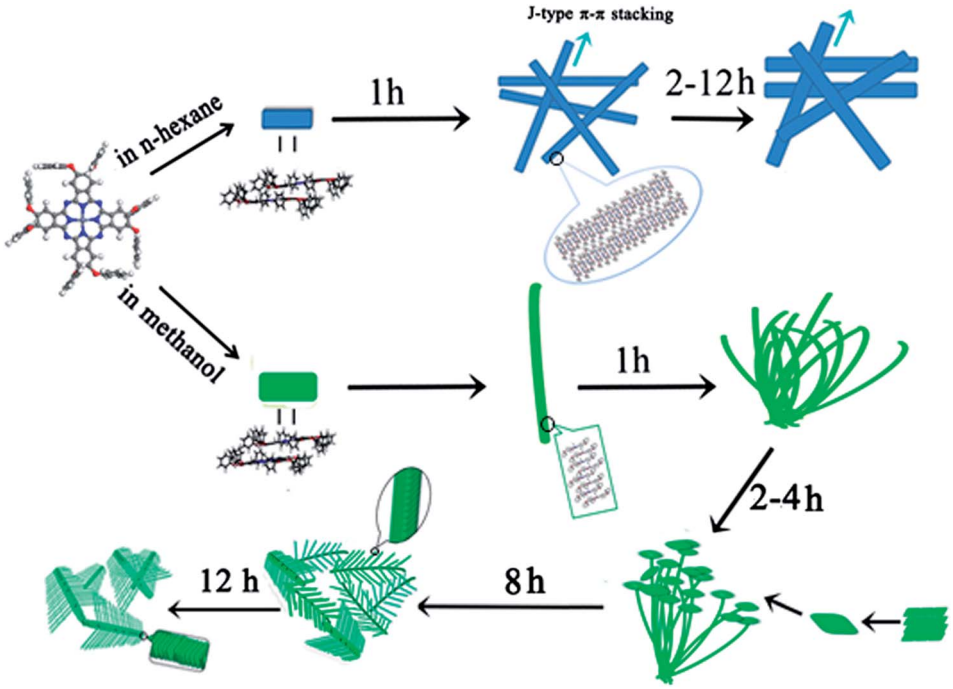

Fig. 6 Schematic illustration for the formation process of nanostructures of the Zn[Pc(OPh)$_8$] in *n*-hexane and methanol.

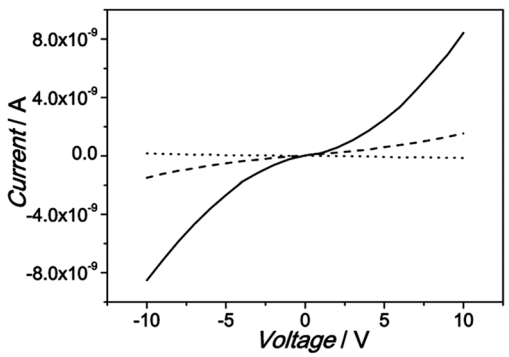

Fig. 7 *I–V* curves measured for nanobelts and nanoleaves of Zn[Pc(OPh)$_8$] formed from *n*-hexane (solid line) and methanol (dash line) and the cast film (dot line) deposited on ITO IDEs/glass substrates.

nanosticks, microscale needle mushroom and pine leaves, can be controllably prepared by means of coordinating and non-coordinating solvents. The driving force for the aggregate formation is proposed to be different intermolecular Zn–O coordination interactions in cooperation with the π–π interaction between phthalocyanine molecules. The *I–V* experimental results revealed that the present Zn[Pc(OPh)$_8$] molecules might serve as the useful functional materials for nano-electronics. Therefore, our results provide a new fundamental insight into the solvent effect on the self-assembly of phthalocyanines. It will be valuable for the design and preparation of phthalocyanine-based nano-electronic and nano-optoelectronic devices with good performance due to the close relationship between the molecular ordering and dimensions of nanostructures and the performance of nanodevices.

Experimental section

Chemicals

DMF were freshly distilled just before use. Column chromatography was carried out on silica gel (Merck, Kieselgel 60, 200–300 with mesh) the indicated eluent.

The 2,3,9,10,16,17,24,25-octakis(phenoxy)phthalocyanine (Zn[Pc(OPh)$_8$]) was synthesized and purified according to published procedures.[42] The detailed synthesis procedures together with the structural characterization are described in the ESI.† All other chemicals and solvents were reagent grade and used as received without further purification.

Characterization

The MALDI-TOF mass spectrum was recorded with a Bruker BIFLEX III ultra-high resolution Fourier transform ion cyclotron resonance (FT-ICR) mass spectrometer by using α-cyano-4-hydroxycinnamic acid as matrix. Electronic absorption spectra were obtained with a Hitachi U-4100 spectrophotometer; fluorescence spectra were measured on an Edinburgh FLS920 at room temperature. Elemental analysis was performed with an Elementar Vario El. IR spectra (KBr pellets) were recorded on a BIORAD FTS-165 spectrometer. SEM images were obtained using a JEOL JSM-6700F field-emission SEM. For SEM imaging, Au (1–2 nm) was sputtered onto the substrate to prevent the charging effects and to improve the image clarity. X-ray photoelectron spectroscopy (XPS) was carried out on a PHI 5300 ESCA System (PerkinElmer, USA). The excitation source is Al$_{K\alpha}$ radiation. X-ray diffraction (XRD) experiment was carried out on a Bruker AXS D8 ADVANCE X-ray diffractometer.

Nanostructure fabrication

The nanostructures of the compound $Zn[Pc(OPh)_8]$ was fabricated by the phase-transfer method according to the following procedure.[43] A minimum volume (50 μL) of concentrated chloroform solution of compound $Zn[Pc(OPh)_8]$ (1 mM) was injected rapidly into a large volume of methanol or *n*-hexane (1 mL), respectively After being kept at room temperature for 1, 2, 4, 8, 12 and 24 h, the aggregates precipitated were then transferred to a carbon-coated grid by pipette for SEM observations.

Electrical experiments

The fundamental electrical measurements were performed using a Hewlett-Packard (HP) 4140B parameter analyzer at room temperature. Current–voltage (*I–V*) curves were registered in the −10 to 10 V voltage range with 1 V increments, starting and finishing at 0 V bias to avoid irreversible polarization effects. All experiments have been conducted at least twice to ensure reproducibility. The interdigitated electrode array is composed of 10 pairs of ITO electrode digits deposited onto a glass substrate with the following dimensions: 125 μm electrode width, 75 μm spacing, 5850 μm overlapping length, and 20 nm electrode thickness. Conductivity, σ, can be calculated by the eqn (1),[13,32]

$$\sigma = \frac{d \times I}{(2n-1) \times L \times h \times V} \quad (1)$$

where d is the interelectrode spacing, I the current, n the number of electrode digits, L the overlapping length of the electrodes, and h the film thickness if it is less than that of the electrodes or the electrode thickness when the film thickness exceeds that of the ITO electrodes.

Acknowledgements

Financial support from the Natural Science Foundation of China (21371073, 21201079), Natural Science Foundation of Shandong Province (ZR2011BZ005) and University of Jinan in China is gratefully acknowledged.

Notes and references

1 (*a*) L. Paterson, P. M. MacDonald, J. Arlt, W. Sibbett, E. P. Bryant and K. Dholakia, *Science*, 2001, **292**, 912–914; (*b*) A. C. Mirkin, L. R. Letsinger, C. R. Mucic and J. J. Storhoff, *Nature*, 1996, **382**, 607–609; (*c*) C. Huang, Y. Li, Y. Song, Y. Li, H. Liu and D. Zhu, *Adv. Mater.*, 2010, **22**, 3532–3536; (*d*) J. A. A. W. Elemans, R. van Hameren, R. J. M. Nolte and A. E. Rowan, *Adv. Mater.*, 2006, **18**, 1251–1226.

2 (*a*) G. Lu, Y. Chen, Y. Zhang, M. Bao, Y. Bian, X. Li and J. Jiang, *J. Am. Chem. Soc.*, 2008, **130**, 11623–11630; (*b*) S. Cui, H. Liu, L. Gan, Y. Li and D. Zhu, *Adv. Mater.*, 2008, **20**, 2918–2925.

3 H. Gan, H. Liu, Y. Li, Q. Zhao, Y. Li, S. Wang, T. Jiu, N. Wang, X. He, D. Yu and D. Zhu, *J. Am. Chem. Soc.*, 2005, **127**, 12452–12453.

4 K. Balakrishnan, A. Datar, T. Naddo, J. Huang, R. Oitker, M. Yen, J. Zhao and L. Zang, *J. Am. Chem. Soc.*, 2006, **128**, 7390–7398.

5 S. Zhang, *Nature biotechnology*, 2003, **21**, 1171–1178.

6 D. M. Vriezema, J. Hoogboom, K. Velonia, K. Takazawa, P. C. M. Christianen, J. C. Maan, A. E. Rowan and R. J. M. Nolte, *Angew. Chem., Int. Ed.*, 2003, **115**, 796–800.

7 (*a*) D. Y. Yan, Y. F. Zhou and J. Hou, *Science*, 2004, **303**, 65–67; (*b*) J.-S. Hu, Y.-G. Guo, H.-P. Liang, L.-J. Wan and L. Jiang, *J. Am. Chem. Soc.*, 2005, **127**, 17090–17095; (*c*) T. Shimizu, M. Masuda and H. Minamikawa, *Chem. Rev.*, 2005, **105**, 1401–1444; (*d*) L. Zhi, T. Gorelik, J. Wu, U. Kolb and K. Müllen, *J. Am. Chem. Soc.*, 2005, **127**, 12792–12793; (*e*) Q. Liu, Y. Li, H. Liu, Y. Chen, X. Wang, Y. Zhang, X. Li and J. Jiang, *J. Phys. Chem. C*, 2007, **111**, 7298–7301; (*f*) Q. Liu, J. Zhu, T. Sun, H. Zhou, Q. Shao, G. Li, X. Liu and Y. Yin, *RSC Adv.*, 2013, **3**, 2765–2769.

8 A. B. P. Lever and C. C. Leznoff, *Phthalocyanine: Properties and Applications*, VCH, New York, 1989–1996, vol. 1–4.

9 N. B. McKeown, *Phthalocyanines Materials: Synthesis, Structure and Function*, Cambridge University Press, New York, 1998.

10 G. de la Torre, G. Bottari, U. Hahn and T. Torres, in *Structure and Bonding: Functional Phthalocyanine Molecular Materials*, ed. J. Jiang, Springer, Heidelberg, 2010, vol. 135, pp. 1–45.

11 K. M. Kadish, K. M. Smith and R. Guilard, *The Porphyrin Handbook*, Academic Press, San Diego, 2000–2003, vol. 1–20.

12 J. Gao, G. Lu, J. Kan, Y. Chen and M. Bouvet, *Sens. Actuators, B*, 2012, **166**, 500–507.

13 Y. Chen, D. Li, N. Yuan, J. Gao, R. Gu, G. Lu and M. Bouvet, *J. Mater. Chem.*, 2012, **22**, 22142–22149.

14 (*a*) Y. Chen, M. Bouvet, T. Sizun, Y. Gao, C. Plassard, E. Lesniewska and J. Jiang, *Phys. Chem. Chem. Phys.*, 2010, **12**, 12851–12861; (*b*) P. Ma, J. Kan, Y. Zhang, C. Hang, Y. Bian, Y. Chen, N. Kobayshi and J. Jiang, *J. Mater. Chem.*, 2011, **21**, 18552–18559.

15 (*a*) Y. Chen, W. Su, M. Bai, J. Jiang, X. Li, Y. Liu, L. Wang and S. Wang, *J. Am. Chem. Soc.*, 2005, **127**, 15700–15701; (*b*) J. Kan, Y. Chen, D. Qi, Y. Liu and J. Jiang, *Adv. Mater.*, 2012, **24**, 1755–1758; (*c*) D. Li, H. Wang, J. Kan, W. Lu, Y. Chen and J. Jiang, *Org. Electron.*, 2013, **14**, 2582–2589.

16 Q. Wang, Y. Li, X. Z. Yan, M. Ropp, D. Galipeau and J. Jiang, *Appl. Phys. Lett.*, 2008, **93**, 073303.

17 Z. Liu, A. A. Yasseri, J. S. Lindsey and D. F. Bocian, *Science*, 2003, **302**, 1543–1545.

18 (*a*) E. A. Luk Centyanets, *J. Porphyrins Phthalocyanines*, 1999, **3**, 424–427; (*b*) H. Ali and J. E. van Lier, *Chem. Rev.*, 1999, **99**, 2379–2450.

19 (*a*) G. Torre, P. Vázquez, F. Agullo-Lopez and T. Torres, *Chem. Rev.*, 2004, **104**, 3723–3750; (*b*) S. Q. Zhou, W. F. Qiu, W. P. Hu, Y. Q. Liu, F. L. Bai and D. B. Zhu, *Thin Solid Films*, 2000, **375**, 263–236.

20 Z. Hao, X. Wu, R. Sun, C. Ma and X. Zhang, *ChemPhysChem*, 2012, **13**, 267–273.

21 J. Kan, Y. Chen, J. Gao, L. Wan, T. Lei, P. Ma and J. Jiang, *J. Mater. Chem.*, 2012, **22**, 15695–15701.

22 H. Engelkamp, S. Middelbeek and R. J. M. Nolte, *Science*, 1999, **284**, 785–788.
23 P. Ma, Z. Bai, Y. Gao, Q. Wang, J. Kan, Y. Bian and J. Jiang, *Soft Matter*, 2011, **7**, 3417–3422.
24 W. Sun, H. Wang, J. Sun, J. Kan, Y. Chen and J. Jiang, *Dyes Pigm.*, 2013, **99**, 154–159.
25 M. Kasha, H. R. Rawls and M. A. EL-Bayoumi, *Pure Appl. Chem.*, 1965, **11**, 371–392.
26 K. Kameyama, M. Morisue, A. Satake and Y. Kobuke, *Angew. Chem.*, 2005, **44**, 4763.
27 D. J. Darwent, P. Douglas, A. Harriman, G. Porter and M. C. Richoux, *Coord. Chem. Rev.*, 1982, **44**, 83–126.
28 X. Huang, F. Zhao, Z. Li, Y. Tang, F. Zhang and C. H. Tung, *Langmuir*, 2007, **23**, 5167–5172.
29 J. Jiang, M. Bao, L. Rintoul and D. P. Arnold, *Coord. Chem. Rev.*, 2006, **250**, 424–448.
30 Y. Gao, Y. Chen, R. Li, Y. Bian, X. Li and J. Jiang, *Chem.–Eur. J.*, 2009, **15**, 13241–13252.
31 Y. Gao, X. Zhang, C. Ma, X. Li and J. Jiang, *J. Am. Chem. Soc.*, 2008, **130**, 17044–17052.
32 (*a*) H. Derouiche, J. C. Bernède and J. L'Hyver, *Dyes Pigm.*, 2004, **53**, 277–289; (*b*) B. Xie, C. C. Finstad and A. J. Muscat, *Chem. Mater.*, 2005, **17**, 1753–1764; (*c*) G. Lu, X. Zhang, X. Cai and J. Jiang, *J. Mater. Chem.*, 2009, **19**, 2417–2424.
33 J. S. Hu, Y. G. Guo, H. P. Liang, L. J. Wan and L. Jiang, *J. Am. Chem. Soc.*, 2005, **127**, 17090–17095.
34 K. E. Martin, Z. Wang, T. Busani, R. M. Garcia, Z. Chen, Y. Jiang, Y. Song, J. L. Jacobsen, T. T. Vu, N. E. Schore, B. S. Swartzentruber, C. J. Medforth and J. A. Shelnutt, *J. Am. Chem. Soc.*, 2010, **132**, 8194–8201.
35 Z. Chen, U. Baumeister, C. Tschierske and F. Würthner, *Chem.–Eur. J.*, 2007, **13**, 450–465.
36 (*a*) H. Ahrens, K. Graf and C. A. Helm, *Langmuir*, 2001, **17**, 3113–3115; (*b*) T. Shimizu, M. Masuda and H. Minamikawa, *Chem. Rev.*, 2005, **105**, 1401–1443.
37 H. Ahn, A. Chandekar, B. Kang, C. Sung and J. E. Whitten, *Chem. Mater.*, 2004, **16**, 3274–3278.
38 Y. Che, A. Datar, K. Balakrishnan and L. Zang, *J. Am. Chem. Soc.*, 2007, **129**, 7234–7235.
39 G. A. O'Brien, A. J. Quinn, D. A. Tanner and G. Redmond, *Adv. Mater.*, 2006, **18**, 2379–2383.
40 Z. Wang, C. J. Medforth and C. J. Shelnutt, *J. Am. Chem. Soc.*, 2004, **126**, 15954–15955.
41 Y. Chen, Y. Feng, J. Gao and M. Bouvet, *J. Colloid Interface Sci.*, 2012, **368**, 387–394.
42 S. E. Maree and T. Nyokong, *J. Porphyrins Phthalocyanines*, 2001, **5**, 782–792.
43 S. Z. Liu, X. Wu, A. Q. Zhang, J. J. Qiu and C. M. Liu, *Langmuir*, 2011, **27**, 3982–3990.